Neuron, Volume *69*

SUPPLEMENTAL INFORMATION

Sun Compass Integration of Skylight Cues in Migratory Monarch Butterflies

Stanley Heinze and Steven M. Reppert

Inventory:

Supplemental Figures

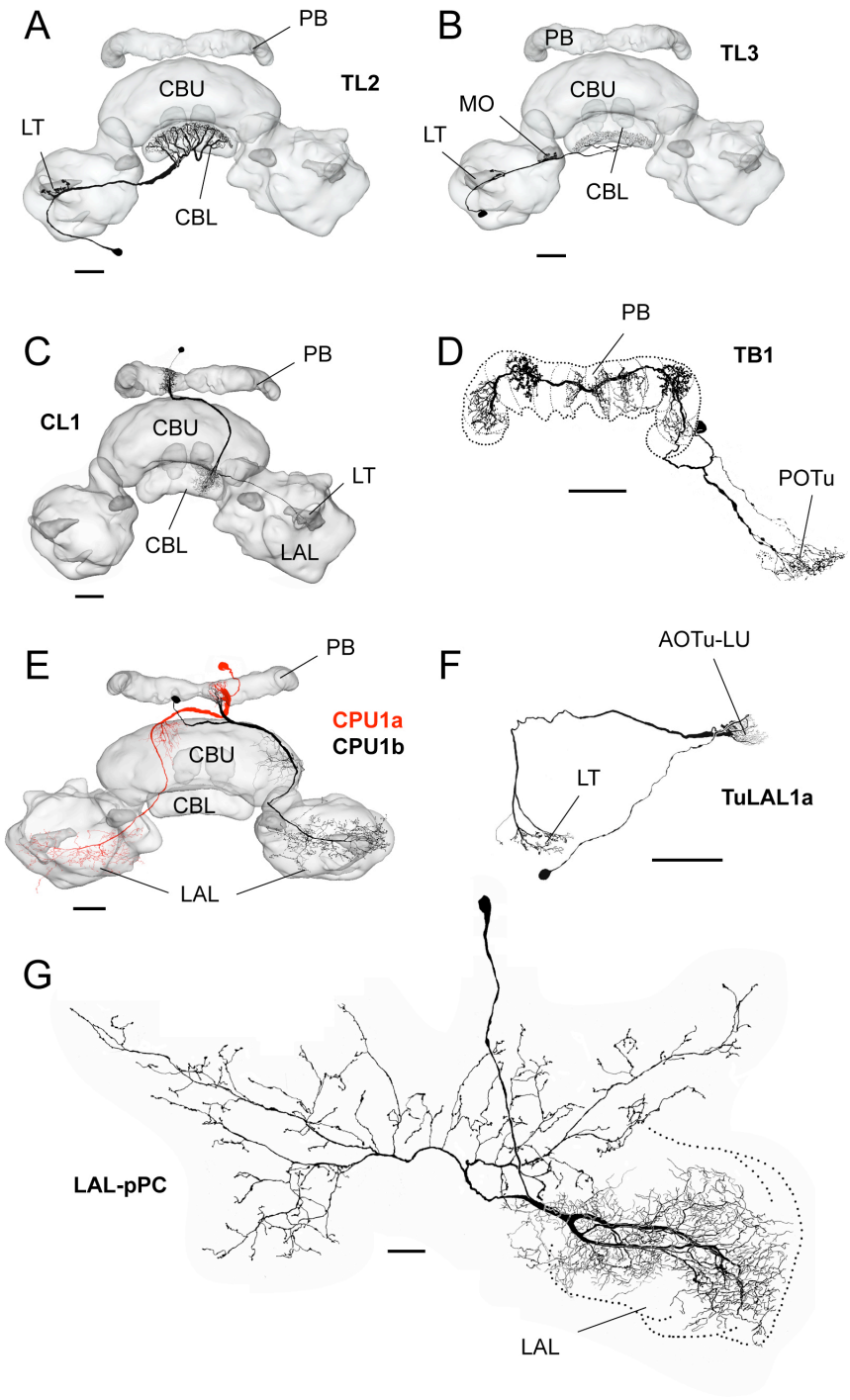

Figure S1, related to Figure 3. Morphology of polarization sensitive neurons of the locust central complex. Cells in each panel (**A-G**) directly correspond to homologue neurons of the monarch butterfly shown in panels of **Figure 3**. All cells are frontal views of two-dimensional camera lucida drawings, additionally projected onto a three-dimensional reconstruction of the central complex and lateral accessory lobes (LAL) in

A,B,C, and **E**. Cell types are indicated as bold abbreviations for each reconstruction. Scale bars represent 50µm.
AOTu-LU, lower unit of the anterior optic tubercle; CBL, lower division of the central body; CBU, upper division of the central body; PB, protocerebral bridge; LT, lateral triangle; MO, medial olive. Images were adapted from Heinze et al. (2009) (**A-D**), Heinze and Homberg (2008) (**E**), Träger et al. (2008) (**F**), and Heinze and Homberg (2009) (**G**).

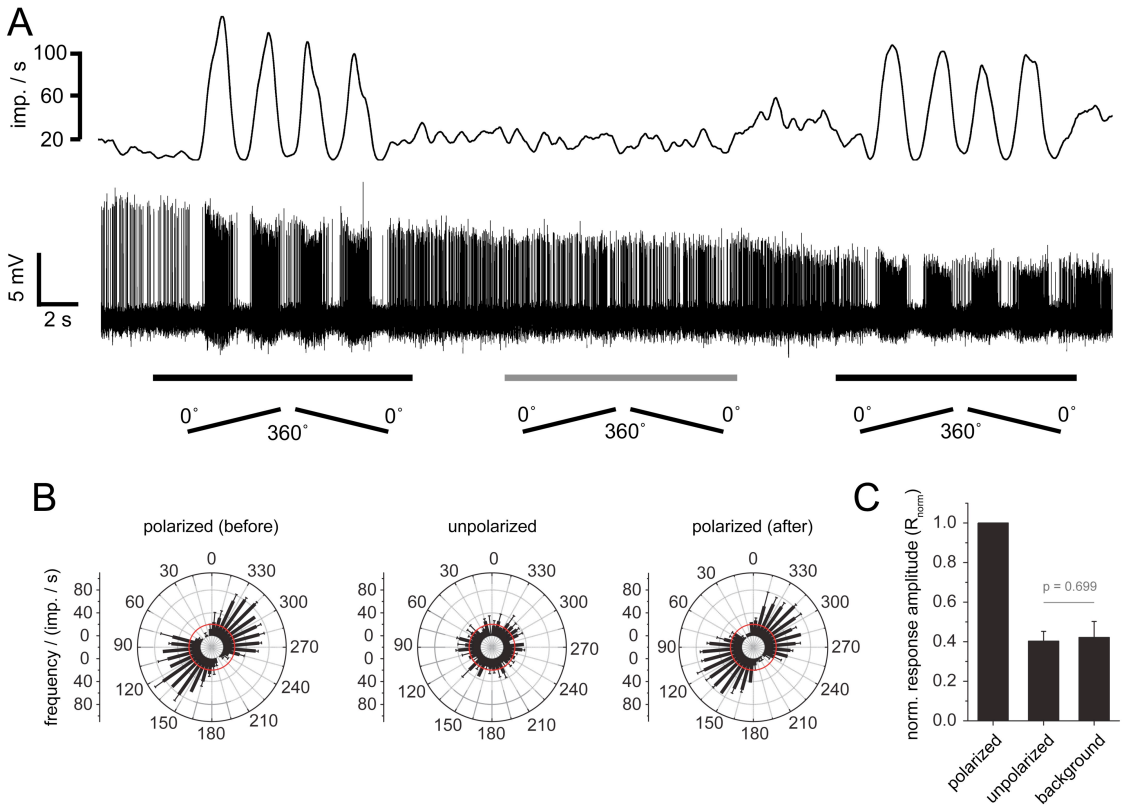

Figure S2, related to Figure 6. Responses of polarization-sensitive neurons to unpolarized, ultraviolet light applied from the zenith. **A,** Raw data of one experimental run (TuLAL-cell). The lower trace shows the spike train, while the upper trace shows the mean spike frequency. Horizontal bars indicate duration of light application (black: polarized light; grey: unpolarized light of equal intensity). Ramps indicate the angular position of the polarizer (rising: clockwise turn; falling: counter clockwise turn). Unpolarized light was produced by placing a diffuser between the polarizer and the butterfly. **B.** Mean spike frequencies plotted against the angular position of the polarizer (bin width: 10˚) for the three stimuli shown in **A** (mean ± SD; n = 2 for each stimulus situation). **C.** Response amplitudes resulting from stimulation with polarized light and unpolarized light compared to background variability (mean ± SE; n = 6). Ultraviolet stimuli were applied from the zenith. Values were normalized to the mean response amplitude of each cell for polarized light stimulation. Responses to unpolarized light were not significantly different from background level (paired t-test). Recorded neurons included one TuLAL, one TL, one CL1, two CPU1a, and one recording with undefined anatomy.

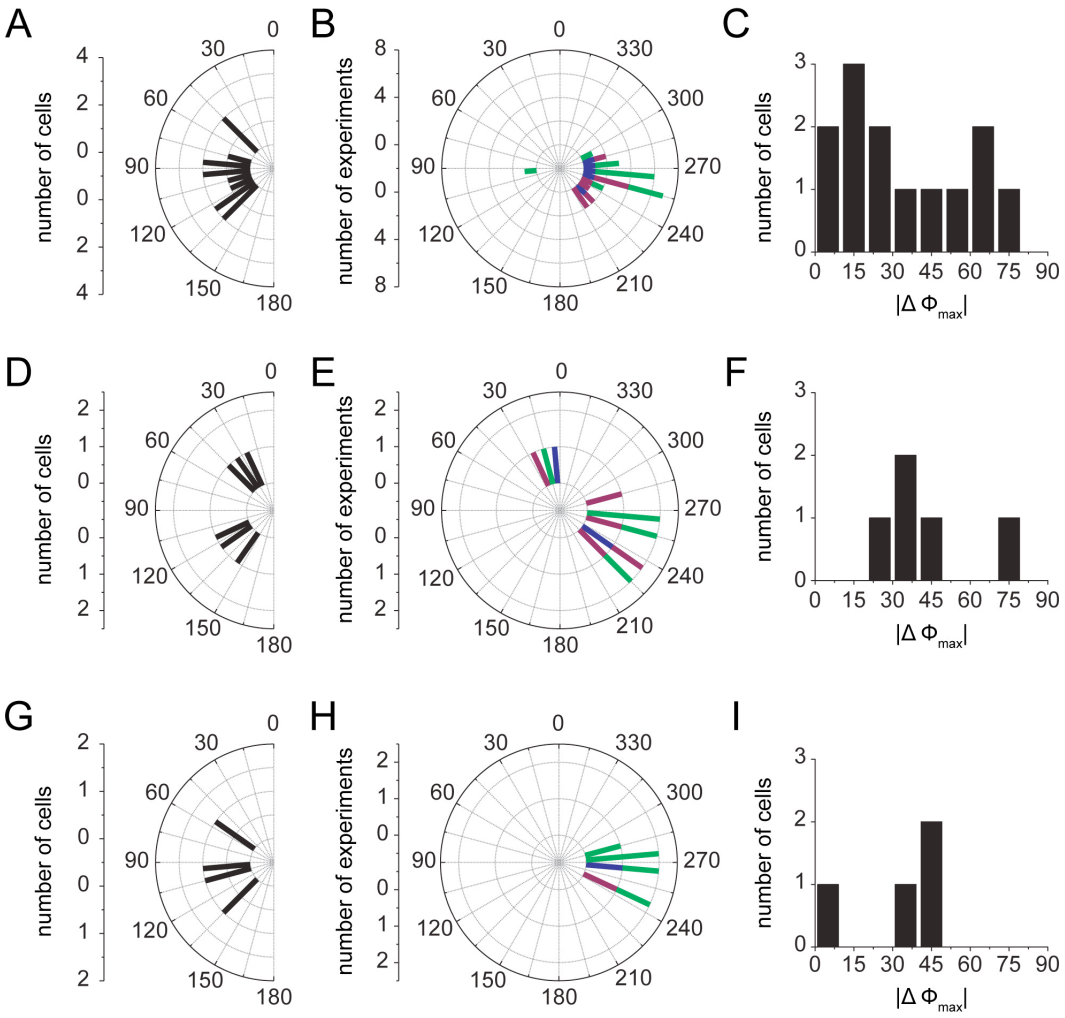

Figure S3, related to Figure 7. *E*-vector tunings and azimuth tunings of different neuron types. **A-C**, TuLAL1 neurons; **D-F**, TL neurons; **G-I**, neurons of unknown morphologies from the same recording site. Left column (**A, D, G**), distributions of Φ_{max}-values. There were no differences between neuronal cell types (Watson-Williams F-test for axial data, $p = 0.308$). Middle column (**B, E, H**), preferred azimuth. Different colors represent experiments using differently colored light spots (green, blue, and ultraviolet [violet]). Comparison of mean azimuth tunings of neurons reveals no difference between the cell types (Watson-Williams F-test for circular data, $p = 0.709$). Right column (**C, F, I**), distributions of absolute difference angles between *E*-vector tuning and mean azimuth tuning for each cell type. None of the distributions was significantly different from a uniform distribution (Kuiper's V-test for axial data, $p > 0.05$ in F, $p > 0.15$ in **C** and **I**; test was performed on doubled values to fit the 180° range of axial data).

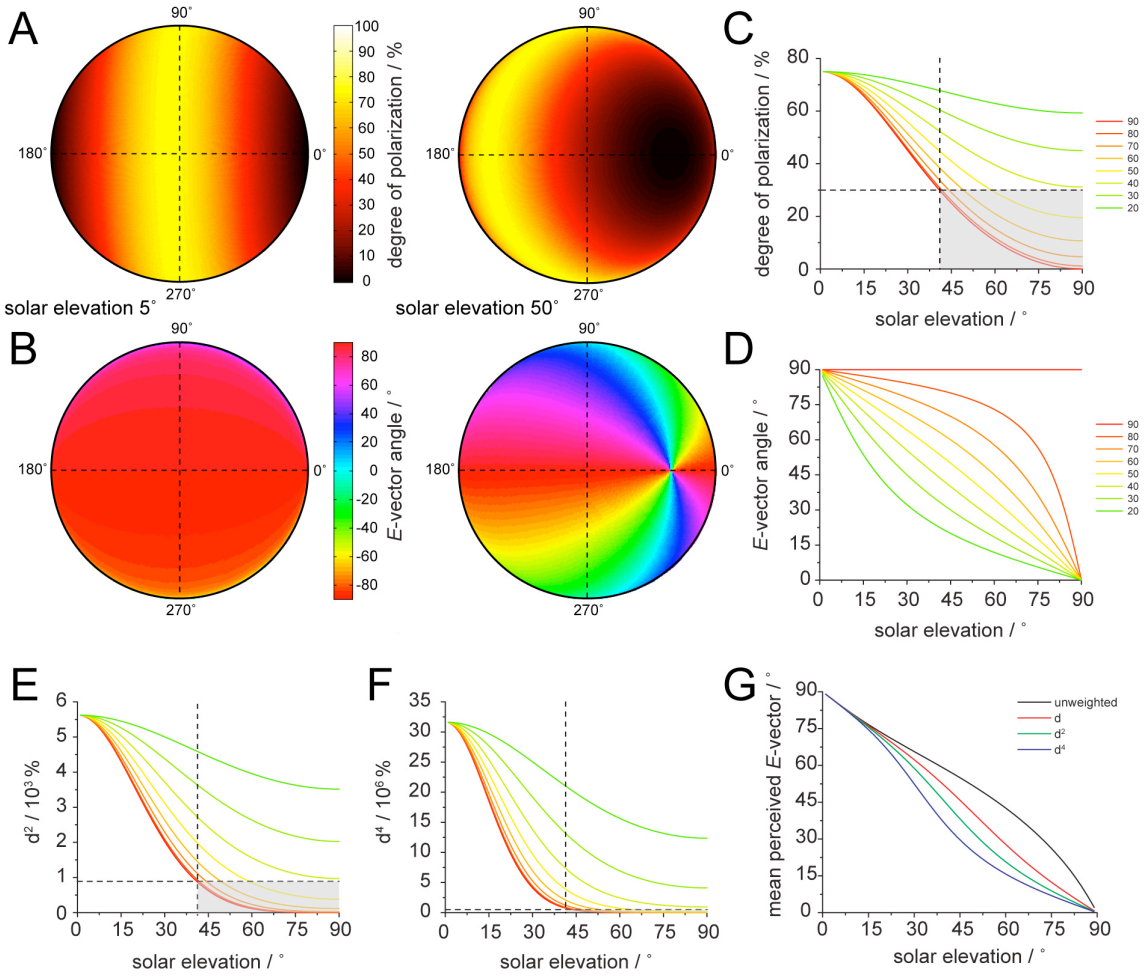

Figure S4, related to Figure 8. A-D, Skylight parameters at different solar elevations. **A,** Degree of polarization in the sky at low solar elevation (5°, left panel) and high solar elevation (50°, right panel). Solar azimuth is defined as 0°; the degree of polarization is lowest close to the sun, and highest 90° away from the sun. **B,** *E*-vector distribution at the sky for low solar elevations (left panel) and high solar elevation (right panel). **C,** Relation between degree of polarization (d) and solar elevation along the 90° azimuth of the sky for different elevations of the observed point (10° steps from 20° to 90°). The degree of polarization is uniformly large throughout the observed sky region at low solar elevations. However, for solar elevations above 40°, high degrees of polarization can only be found near the horizon along the observed azimuth. Although the *E*-vector angle in the observed sky area is the information relevant for the butterfly, as it contains information about solar position, the utilization of this information is limited by the degree of polarization at the observed point. The grey shaded area indicates degrees of polarization, which we defined as unusable (below 30%) for the butterfly based on data from the desert locust (Pfeiffer et al., 2011). **D,** Relation of *E*-vector angle and solar elevation along the 90° azimuth of the sky, calculated for different elevations of the observed point (10° steps from 20° to 90°). The *E*-vector angle changes with solar elevation throughout the observed region (with the exception of the zenith), but at

different rates, depending on the elevation of the observed point. Thus, the DRA is exposed to a mixture of different *E*-vector angles, which additionally change over the course of the day. To simplify this complex relationship, an integrated version of skylight parameters across the DRA receptive field was calculated for each given solar elevation (mean perceived *E*-vector).

E & F, Development of the weighting function for averaging *E*-vector angles along the 90° azimuth at different solar elevations. To eliminate *E*-vectors at points in the sky with values of d lower than 30% from the averaging process, a weighting function had to be introduced. First, d itself was used to weigh the importance of *E*-vectors at each observed point in the sky (**C**). Although points with low values of d had less influence on the result of the average, regions below 30% were still not eliminated. Thus, d^2 functions (**E**) and d^4 functions (**F**) were calculated to subsequently reduce the influence of values below 30% to near zero (indicated be the grey shaded area). The function depicted in **F** was eventually used as the final weighting function, as it eliminated irrelevant regions of the sky for calculating the mean perceived *E*-vector. In sum, the average perceived *E*-vector over the course of the day was used as an estimate of overall information relayed from the DRA that is available to the recorded neurons at different daytimes.

G, Effect of different weighting functions on the mean perceived *E*-vector function. The graph shows the relation between the mean perceived *E*-vector and solar elevation. This function was calculated by averaging the *E*-vectors in all parts of the sky viewed by the dorsal rim area of the compound eye (different elevations along the 90° azimuth). The raw axial average for all solar elevations is shown by the black line (unweighted). When different parts of the sky were weighted differentially during the averaging process, the resulting values changed according to the weighting function. Resulting functions are shown for weighting each *E*-vector with its associated degree of polarization (d, red), d^2 (green), and d^4 (blue). Note that all functions lead to similar results for low solar elevations, as values of d are more uniformly distributed in the sky, but differ markedly towards higher solar elevations (d in the vicinity of the sun is low).

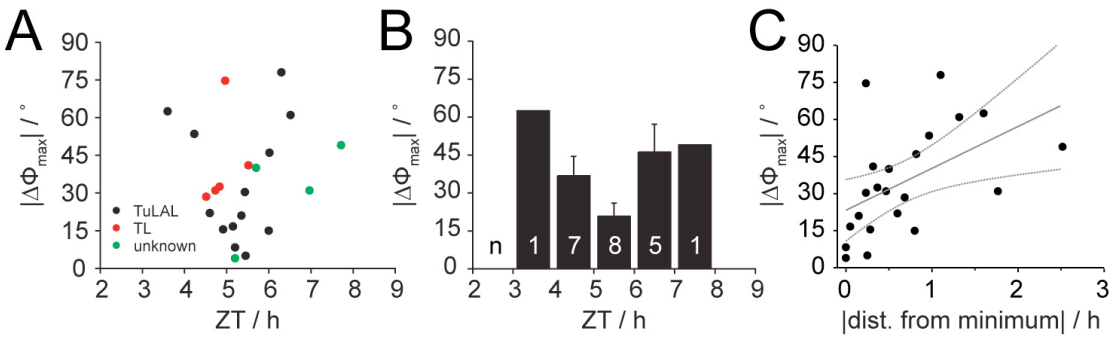

Figure S5, related to Figure 8. Relationship of the variability of *E*-vector tuning and the time of day of recording. **A,** Although all intracellular recordings were aimed at ZT 5, the actual range of recording times varied from ZT 3.6 to ZT 7.7, thereby covering four hours of the 11-hour light period. When plotting $\Delta\Phi_{max}$-values against recording time, it was apparent that large values were most common in the early (near ZT 3.6) recording and late (near ZT 7.7) recording, while small values were clustered around ZT 5. ZT 0 = lights on. **B,** Same data as **A** but grouped at one-hour intervals (mean ± SE). **C**, Regression analysis between $\Delta\Phi_{max}$-values and their respective recording times before and after ZT 5.2 (time point with smallest $\Delta\Phi_{max}$-value) revealed a significant relationship ($p = 0.016$).

Supplemental Experimental Procedures

Animals

Migrating monarch butterflies were captured in the wild from roosts between October 29-31, 2009. They were caught either in St. Mark's Wildlife refuge (near Tallahassee, Florida) or near Port Lavaca, Texas. After shipping to Worcester (MA), they were kept in the laboratory in glassine envelopes in Percival incubators with controlled light and temperature cycles imitating fall conditions (11 h light:13 h dark; light, 23º C:dark, 12º C) at 70% humidity. They were fed a 25% honey solution every other day. As monarch butterflies migrate during the daytime, recordings in migrants were performed around ZT 5, the midpoint of their normal flight time (from November 3, 2009 until March 2, 2010). Non migratory, summer monarch butterflies obtained from Fred Gagnon, Greenfield, Massachusetts, were used for initial recordings and the control experiments in Figure S2 using unpolarized zenithal light stimulation. These animals were also housed in glassine envelopes, and maintained in a 12 h light:12 hour dark cycle at 25˚C and fed as described above.

Immunocytochemistry

For immunocytochemical labeling of neuropils animals were decapitated and the brain was dissected in physiological saline. After fixation in 4% paraformaldehyde/0.1 M phosphate buffer (pH 7.4) at room temperature for 3 hours, brains were rinsed 4 x 15 min in 0.1 M phosphate buffered saline (PBS; pH 7.4). The ganglionic sheath was made permeable by treatment with 1 mg/ml collagenase-dispase (in PBS, pH 7.4) for 1 h. Following another washing step (4 x 15min PBS), the brains were preincubated overnight with 5% normal goat serum (NGS) in PBS containing 0.3% TritonX (PBT) at 4°C. To visualize neuropil structures, the brains were incubated with a monoclonal antibody against the synaptic protein synapsin (SYNORF1, developed by E. Buchner (Klagges et al., 1996, obtained from the Developmental Studies Hybridoma Bank, University of Iowa) diluted at 1:50 in PBT containing 1% NGS for 5 days at 4°C. The brains were then washed 6 x 20 min with PBT. Secondary antibody (Cy5-conjugated goat anti mouse; Jackson Immunoresearch, Westgrove, Pa.) was used at a dilution of 1:300 in PBT

containing 1% NGS for to 3 days at 4°C. After washing 3 x 20 min in PBT and 2 x 20 min in PBS, brains were dehydrated in an increasing ethanol series (25%, 50%, 70%, 90%, 95%, 100%, 15 min each), prepared for clearing in a solution of 50% ethanol/50% methyl salicylate, and cleared with methyl salicylate (30 min). Finally, the brains were mounted in Permount (Fisher Scientific, Pittsburgh, Pa.) between two glass cover-slides separated by spacing rings to avoid squeezing.

Image Acquisition and Three-Dimensional Neuropil Reconstructions

Confocal image stacks were obtained either with a 10x air objective or with a 25x oil immersion objective (LD LCI Plan-Apochromat 25x/0.8 Imm Corr DIC; Zeiss). Low resolution images (10x; final voxel size: 3µm³) were used for reconstruction of the complete brain, while high resolution stacks were used for reconstruction of the central complex (25x; final voxel size 1µm³). To capture the whole brain, six partly overlapping image stacks (three from anterior and three from posterior) had to be obtained and later recombined and merged in Amira5.0 software (Mercury Computer Systems, San Diego, CA). The axial distortion due to refractory mismatch when using an air objective was compensated by scaling the resulting image stacks in the z-direction by a factor of 1.49 (determined by comparing z-dimensions of data obtained with oil- and air objective from the same brain regions of the identical preparation). The final voxel size was reached by down sampling the confocal image data, particularly in the x- and y-dimensions. This was necessary to allow further processing with the available PC-hardware.

For reconstruction, neuropil areas of interest were first labeled with the segmentation editor in Amira5.0. During this procedure, selected voxels were assigned to particular neuropils, resulting in a volumetric dataset called the label field. The reconstruction of polygonal surface models was then automatically achieved on the basis of these label fields. The used color code is based on the standard atlases of the brain of the honey bee, the desert locust, and the hawkmoth (Brandt et al., 2005, Kurylas et al., 2008; el Jundi et al., 2009).

Histology for Neurobiotin Injections

After injection of Neurobiotin, brains were dissected out of the head capsule, cleaned of fat and trachea, and fixed overnight at 4°C in Neurobiotin fixative (4% paraformaldehyde, 0.25% glutaraldehyde, 2% saturated picric acid, in 0.1 M phosphate buffer). Brains were then transferred to 0.1M phosphate buffer and stored up to one week. For further processing, the brains were rinsed 4 x 15 min in PBS, and incubated with Cy3-conjugated Streptavidin (Rockland; 1:1000) for 3 d at 4°C in PBT (PBS, including 0.5% Triton X-100). After rinsing with PBT (3 x 20 min) and PBS (2 x 20 min), an increasing ethanol series (25, 50, 70, 90, 95, and 100%; 15 min each) was used for dehydration of the brains, which were then transferred to a fresh mixture of ethanol and methyl salicylate (1:1) for 15 min, and finally cleared in methyl salicylate for 30 min. Brains were eventually mounted in Permount (Fisher Scientific) between two coverslips. To avoid compressions, reinforcement rings were used as spacers.

Neuron Reconstruction

Two-dimensional reconstructions of single neurons were based on neurobiotin injected cells. Confocal image stacks were acquired with the 25x objective. Several stacks were required to capture all regions of a neuron. These image stacks were directly loaded into Photoshop software (version CS2) as multilayer images. Reconstruction of neuronal arborizations present in each individual layer was carried out in a common overlaying, transparent layer using the pencil tool. The resulting two dimensional, frontal projection views of each confocal image stack were then merged into one image. According to neuropil boundaries visible from background staining, this image was finally projected onto a three dimensional reconstruction of the central-complex neuropils.

Three-dimensional reconstructions of single neurons were based on dye injected wholemount preparations. Confocal image stacks were captured and processed analogous to high resolution image stacks for neuropil reconstruction. However, data stacks did not have to be merged, but could remain separate after they had been aligned to their correct spatial positions. This allowed data to be used without down sampling in the original high resolution quality. The reconstruction of the neurons was achieved by using a supplemental tool for Amira4.2 as described by Schmitt et al. (2004), with a diameter-

and midline-fitted skeleton tree being the finally presented dataset. The updated version of this tool was kindly provided by J.F. Evers (Cambridge, UK). For providing neuropil reconstructions from the dye injected brains, unspecific background staining was used analogous to anti-synapsin staining.

Electrophysiology

For recordings, animals were waxed onto a plastic holder. Legs and wings were removed and the head capsule was opened fronto-dorsally. The brain was freed of surrounding trachea and fat body. Most muscles in the head capsule were transected and removed. Recordings were all performed on the left side of the brain. To access the recording site the left antenna was removed, while it was left intact on the right side. To increase stability, the esophagus was transected and the gut was removed from the opened abdomen, which was resealed using a tightly knotted thread. To facilitate electrode penetration, the neural sheath was locally removed with forceps after brief digestion by application of Pronase powder (30s; Roche) and intense rinsing with ringer solution (150mM NaCl, 3mM KCl, 10mM TES, 25mM sucrose, 3mM $CaCl_2$; pH = 6.9; King et al., 2000). The animal was then mounted in the recording setup, with the vertical axis of the compound eye aligned horizontally. Thus the dorsal side of the eye faced the stimulation setup, while the recording electrode could be inserted vertically from the frontal side without obscuring the dorsal field of view. An additional silver wire inserted into the abdomen was used as reference electrode. Desiccation was prevented by keeping the brain submerged in ringer solution.

Intracellular recordings were performed with sharp electrodes (resistance 60–150 MΩ), drawn from borosilicate capillaries (inner diameter, 0.75 mm; outer diameter, 1.5 mm; Sutter) using a Flaming/Brown horizontal puller (P-97, Sutter). Electrode tips were filled with 4% Neurobiotin (Vector Laboratories) dissolved in 1 M KCl and backed up with 1 M KCl. Intracellular signals were amplified (10x) with a SEC05-LX amplifier (NPI; amplifier set to bridge mode). After sampling at a sampling rate of 5 kHz (CED1401 Micro, Cambridge Electronic Design), signals were stored on a PC using Spike2-software (Cambridge Electronic Design). Digital high pass filtering was applied when necessary to compensate for drifting baseline. After completion of the stimulation

protocols, depolarizing current was applied (1–3 nA, 1–5 min) to iontophoretically inject Neurobiotin when stability of recording allowed.

Visual Stimulations

Two different types of visual stimuli were applied during the experiments. First, linearly polarized light was presented from the zenith (as seen by the animal). Second, unpolarized light spots were presented at an elevation of 25°-30° (above the animal's horizon). Both stimuli were connected to a rotation stage (Micos DT-50-DC), which could be rotated by 360° in either direction. Through a central hole in the rotation stage, light from a light emitting diode (LED, ultraviolet, 365 nm emission peak) was passed via a polarization filter (BVO-UV, Boldervision). The angular size of the stimulus was 19° with a photon flux rate at the animal's head of 3.1×10^{13} photons/s·cm². During each rotation the plane of polarization was rotated by 360° (0° defined as the *E*-vector parallel to the longitudinal body axis of the animal). The LEDs for unpolarized stimulation (ultraviolet, green, blue) were attached to the rotation stage via radial arms extending from the zenith, so that each LED pointed towards the animal (angular size: 3°). With every rotation, each LED passed through all possible azimuth directions at constant elevation. The LEDs used were either hexagonal high power UV-LEDs (H2A1-H365, peak emission at 365 nm; Roithner) for polarized light and ultraviolet unpolarized light, or Luxeon™ Star green and blue LEDs (LXHL-MB1D, LXHL-MM1D, peak emission at 520 nm and 460 nm, respectively; Roithner). They were driven by a programmable regulated power source (Agilent E3616A), commanded by Spike2 software via an analogue output channel of the digitizer (CED1401 micro). LEDs were driven at maximum current (350 mA) for ultraviolet light, while green and blue LEDs were down regulated to adjust for equal photon flux rate by adjustment of the current (2.3×10^{14} photons/s·cm² at animal's head for unpolarized stimuli). The rotation stage was programmed via a controller (Micos Moco-DC) that provides an RS-232 interface to a PC and its own scripting language, which is directly accessible through a custom made MatLab script. Via this script rotation velocity and rotation direction could be freely adjusted. Over the course of experiments, rotation velocity was either set to 30°/s or

60°/s, and both clockwise as well as counter-clockwise rotations were applied in direct sequence.

For blocking light to the dorsal region of the compound eye, a small piece of black tape, held by a thin glass capillary, was positioned directly in front of the eye by a micromanipulator. Identical stimuli were applied before, during and after the shielding.

To eliminate polarization during control experiments with zenithal unpolarized light, a diffuser (tracing paper, 41g/m^2, Strathmore) was inserted into the light path . Residual polarization during 360˚ rotations of the polarizer/diffuser was estimated by measuring intensity fluctuations after inserting a second, non-rotating polarizer into the light path, and found to be below 5%. Intensity of polarized light was adjusted to match the unpolarized light intensity resulting from insertion of the diffuser.

Analysis of Electrophysiological Data

Neuronal responses to rotations of the polarizer as well as to azimuthal rotations of unpolarized light spots were analyzed with custom designed scripts in Spike2 software. Spikes were first detected by thresholding the voltage signal. Then, each spike occurring during a rotation was assigned its corresponding angle (either *E*-Vector or azimuth). These lists of angles were tested for significant difference from randomness in Oriana3.0 software (Kovach Computing Services) using the Rayleigh test for axial (*E*-vector angles) or circular data (azimuth angles; significance levels 0.05). If activity during rotations was significantly different from randomness, the resulting mean angle was defined as the preferred *E*-vector or azimuth angle of the examined neuron. For illustration purposes, spiking activity during rotations was calculated for 10° bins, averaged over all rotations within each neuron, and plotted against *E*-vector orientation or azimuth angle respectively.

The response amplitude (R) was calculated as described in Heinze et al. (2009). In brief, R is a measure for the summed absolute deviation from mean activity during stimulus application. Thus, the higher the value of R, the stronger is the response to the stimulus. R-values for periods without stimulation were obtained to calculate background variability.

Statistical comparison between shielded and unshielded stimulus conditions were performed by analyzing R-values for each of the conditions (using GraphPad Prism 5 software). First, R-values were normalized to the unshielded response value. A paired t-test was then used to compare the shielded response to background variability (significance level: 0.05), while a one-sample t-test against a hypothetical mean of 1 was performed to compare the shielded response against the normalized unshielded response (significance level: 0.05). Significance of pairing and test for deviations from normal distributions were automatically carried out by the software.

All analysis on population data of preferred neuronal tuning directions were performed with Oriana3.0 (references for all tests: Batschelet, 1981; Zar, 2007). Tests were adjusted for axial data when *E*-vector tunings were analyzed, while tests for circular data were applied for azimuth tunings (all significance levels: 0.05). Distributions of preferred tuning directions were compared with the Watson-Williams F-test, if data were independent (comparison of neuron types), or the Watson U^2-test, if data were not independent (spectral tunings of the same neurons). Significant deviation from randomness of each population of tunings was tested with the Rayleigh-test. Mean azimuth tunings were calculated by calculating the circular mean and SD of individual color tunings. The difference angle between *E*-vector tuning and mean azimuth tuning was defined as the absolute value of the smaller of the two difference angles, so that the resulting values covered a possible range of 90°. The difference angles between responses to individual colors were defined analogous (resulting range: 180°). Finally, the distributions of difference angles were tested for significant deviations from a uniform distribution with the Kuiper's V-test for axial data. Data with a total range of 90° were doubled before the analysis, in order to fit the 180° range of axial data (analogous to transformation of axial data in Oriana).

Regression analysis between $\Delta\Phi_{max}$-values and the absolute deviation in their recording time from ZT5.2 (recording time with minimal $\Delta\Phi_{max}$-value) was performed in GraphPad Prism 5. The slope of the regression was tested for significant deviation from zero (significance level 0.05).

The changes of mean frequency over time were used to visualize the broad response characteristics of recorded neurons. It was calculated by applying a lowpass

filter to the instantaneous frequency (window width 0.5 s) obtained from a spike train (using MatLab).

Generally, standard deviation of the mean (SD) was calculated when the variation of the data was important, while standard error of the mean (SE) was calculated when the precision of the mean was evaluated. For circular data, the SD reflects the circular standard deviation, which is based on the length of the mean vector.

Assessment of Recording Quality

Generally, all recordings have been performed to the same standards as established for similar experiments in the desert locust (Heinze and Homberg, 2007, 2009; Heinze et al., 2009) and covered similar ranges of spike amplitudes and recording durations. Whether a particular recording was chosen for iontophoretic dye injection and/or further analysis, was decided upon stability of the recording and the occurring firing patterns. A recording was disregarded if its baseline fluctuated substantially (e.g. because of movement of the preparation) or when the cell exhibited persistent, very regular firing at high frequencies, indicating massive sodium influx due to injury caused by the recording electrode. Visual stimulation was started as soon as the neuron had reached a stable baseline firing rate after insertion of the electrode. Cell type specific firing patterns were reconfirmed after the recording by evaluation of interspike interval diagrams.

Due to the large depth of the recording site, minute diameter of recorded neurites, and some residual movement in the preparation, the average recording duration was 3 min 35 sec (excluding neurobiotin injection). Additionally, intermittent and unpredictable clogging of the electrode tip (small diameter, high resistance electrodes) prevented precise resistance compensation of the electrode and thus limited our ability to determine the input resistance of the recorded cells, while fluctuating baseline prior to penetration of the neurite prevented accurate measurement of resting potentials. As this limits our ability to comprehensively judge the recording quality, slightly depolarized states of a neuron might remain undetected during the recording. This could result in increased background firing rates and less complete silencing during inhibitory responses (also reported for the cricket, Sakura et al., 2008). Because of this, no conclusions are based on these characteristics, as they only become reliable with large numbers of recordings

(Heinze et al., 2009). All major conclusions are solely based on preferred orientations and *E*-vector tunings, which are unlikely to be influenced by even large fluctuations in recording quality. For instance, strongly depolarized neurons (e.g. during current application during dye injection), but also hyperpolarized neurons, show identical *E*-vector tuning compared to before and after current application (unpublished observation of S.H. in the locust).

Modeling

Skylight features of the relevant part of the sky were calculated using the single scattering Rayleigh model (Coulson, 1988), following the implementation by Pfeiffer et al. (2011) and Pfeiffer and Homberg (2007) (see below).

For determining the skylight parameters available to the monarch, the degree of polarization (d) and the *E*-vector angle (Φ) were calculated for different elevations along the 90° azimuth (in steps of 10°, between 20° and 90° elevation). First, results for all possible solar elevations were calculated (resolution 1°; Supplementary Fig. S2C & D). Next, the average *E*-vector angle (Φ_{mean}) across the observed region was determined for any given solar elevation. Hereby, d^4 was used as a weighting factor in order to eliminate degrees of polarization less than 30% (Supplementary Fig. S3). As *E*-vectors are axial values (repeating every 180°), they had to be converted to circular range before averaging. After calculation of the weighted mean, data were back-transformed to the original range. These operations, including the calculation of the weighted mean, were performed with the circular statistics toolbox in Matlab (Berens, 2009).

After Φ_{mean} was calculated for each possible solar elevation, its value was determined for different solar elevations over the course of the day at the capture sites (at date of capture) of the used butterflies. Data for solar elevation values (resolution 10 minutes) were obtained from the US Naval Observatory (USNO) website (http://www.usno.navy.mil/USNO/astronomical-applications/data-services/alt-az-us). The time of sunrise was set to ZT0.

Calculation of Skylight Parameters

As described by Pfeiffer and Homberg (2007), the position of the sun ($\vec{s}$) and the observed spot at the sky ($\vec{o}$) can be described as vectors. As we define the solar azimuth as zero, the observed points lie on the 90° azimuth. The vectors can then be described as functions of the solar elevation (α_s) and the elevation of the observed point (α_o):

$$\vec{s} = \begin{pmatrix} s_1 \\ s_2 \\ s_3 \end{pmatrix} = \begin{pmatrix} \sin(90° - \alpha_s) \\ 0 \\ \cos(90° - \alpha_s) \end{pmatrix} \quad (1)$$

$$\vec{o} = \begin{pmatrix} o_1 \\ o_2 \\ o_3 \end{pmatrix} = \begin{pmatrix} 0 \\ \sin(90° - \alpha_o) \\ \cos(90° - \alpha_o) \end{pmatrix} \quad (2)$$

As skylight parameters at any point $\vec{o}$ depend on its angular distance to the sun, the angle between the sun and the observed points (θ) was determined as the angle between $\vec{s}$ and $\vec{o}$:

$$\theta = \arccos\left(\frac{\vec{s} \cdot \vec{o}}{|\vec{s}| \cdot |\vec{o}|}\right) \quad (3)$$

The degree of polarization (d) was determined according to Pfeiffer et al. (2011):

$$d = 0.75 \cdot \frac{1 - \cos^2(\theta)}{1 + \cos^2(\theta)} \quad (4)$$

The *E*-vector angle (Φ) was determined as the angle of the vector product between $\vec{s}$ and $\vec{o}$ (Pfeiffer and Homberg, 2007):

$$\vec{e} = \vec{s} \times \vec{o} \quad (5)$$

Transformation of the equation leads to:

$$\phi = \arctan\left(\frac{e_2}{e_1}\right) = \arctan\left(\frac{s_3 \cdot o_1 - s_1 \cdot o_3}{s_2 \cdot o_3 - s_3 \cdot o_2}\right) \quad (6)$$

Hereby, e_1 and e_2 are vector components of the *E*-vector ($\vec{e}$). The values of d and Φ were then used to model the information available to the DRA at any given time during the day.

Skylight parameters for the whole sky at any given solar elevation (Figure S2A,B) were calculated using the more general descriptions of $\vec{s}$ and $\vec{o}$ as in Pfeiffer and Homberg (2007). Both, implementation of functions and plotting of results were achieved with a custom designed Matlab-script.

Supplemental References

Batschelet, E. (1981). Circular Statistics in Biology. (London: Academic Press).

Berens, P. (2009). CircStat: A MATLAB toolbox for circular statistics. Journal of Statistical Software *3*.

Brandt, R., Rohlfing, T., Rybak, J., Krofczik, S., Maye, A., Westerhoff, M., Hege, H., Menzel, R. (2005). Three-dimensional average-shape atlas of the honeybee brain and its applications. J. Comp. Neurol. *492,* 1-19.

Klagges, B.R., Heimbeck, G., Godenschwege, T.A., Hofbauer, A., Pflugfelder, G.O., Reifegerste, R., Reisch, D., Schaupp, M., Buchner, S., Buchner, E. (1996) Invertebrate synapsins: a single gene codes for several isoforms in *Drosophila*. J. Comp. Neurol. *16*, 3154-3165.

Kurylas, A. E., Rohlfing, T., Krofczik, S., Jenett, A., Homberg, U. (2008). Standardized atlas of the brain of the desert locust, *Schistocerca gregaria*. Cell Tissue Res. *333,* 125-145.

Zar, J. H. (2007). Biostatistical Analysis. (Englewood Cliffs, NJ: Prentice-Hall).